# A Measurement of the Rate of Charm Production in W Decays

## The OPAL Collaboration

### Abstract

Using data recorded at centre–of–mass energies around 183 GeV and 189 GeV with the OPAL detector at LEP, the fundamental coupling of the charm quark to the W boson has been studied. The ratio $R_{\text{c}}^{\text{W}} \equiv \Gamma\left(\text{W} \rightarrow \text{c X}\right)/\Gamma\left(\text{W} \rightarrow \text{hadrons}\right)$ has been measured from jet properties, lifetime information, and leptons produced in charm decays. A value compatible with the Standard Model expectation of 0.5 is obtained: $R_{\text{c}}^{\text{W}} = 0.481 \pm 0.042\,(\text{stat.}) \pm 0.032\,(\text{syst.})$. By combining this result with measurements of the W boson total width and hadronic branching ratio, the magnitude of the CKM matrix element $|V_{\text{cs}}|$ is determined to be $|V_{\text{cs}}| = 0.969 \pm 0.058$.

(Submitted to Physics Letters B)

# The OPAL Collaboration

G. Abbiendi[2], K. Ackerstaff[8], C. Ainsley[5], P.F. Åkesson[3], G. Alexander[22], J. Allison[16],
K.J. Anderson[9], S. Arcelli[17], S. Asai[23], S.F. Ashby[1], D. Axen[27], G. Azuelos[18,a], I. Bailey[26], A.H. Ball[8],
E. Barberio[8], R.J. Barlow[16], S. Baumann[3], T. Behnke[25], K.W. Bell[20], G. Bella[22], A. Bellerive[9],
G. Benelli[2], S. Bentvelsen[8], S. Bethke[32], O. Biebel[32], I.J. Bloodworth[1], O. Boeriu[10], P. Bock[11],
J. Böhme[14,h], D. Bonacorsi[2], M. Boutemeur[31], S. Braibant[8], P. Bright-Thomas[1], L. Brigliadori[2],
R.M. Brown[20], H.J. Burckhart[8], J. Cammin[3], P. Capiluppi[2], R.K. Carnegie[6], A.A. Carter[13],
J.R. Carter[5], C.Y. Chang[17], D.G. Charlton[1,b], P.E.L. Clarke[15], E. Clay[15], I. Cohen[22], O.C. Cooke[8],
J. Couchman[15], C. Couyoumtzelis[13], R.L. Coxe[9], A. Csilling[15,j], M. Cuffiani[2], S. Dado[21],
G.M. Dallavalle[2], S. Dallison[16], A. de Roeck[8], E. de Wolf[8], P. Dervan[15], K. Desch[25], B. Dienes[30,h],
M.S. Dixit[7], M. Donkers[6], J. Dubbert[31], E. Duchovni[24], G. Duckeck[31], I.P. Duerdoth[16],
P.G. Estabrooks[6], E. Etzion[22], F. Fabbri[2], M. Fanti[2], L. Feld[10], P. Ferrari[12], F. Fiedler[8], I. Fleck[10],
M. Ford[5], A. Frey[8], A. Fürtjes[8], D.I. Futyan[16], P. Gagnon[12], J.W. Gary[4], G. Gaycken[25],
C. Geich-Gimbel[3], G. Giacomelli[2], P. Giacomelli[8], D. Glenzinski[9], J. Goldberg[21], C. Grandi[2],
K. Graham[26], E. Gross[24], J. Grunhaus[22], M. Gruwé[25], P.O. Günther[3], C. Hajdu[29], G.G. Hanson[12],
M. Hansroul[8], M. Hapke[13], K. Harder[25], A. Harel[21], M. Harin-Dirac[4], A. Hauke[3], M. Hauschild[8],
C.M. Hawkes[1], R. Hawkings[8], R.J. Hemingway[6], C. Hensel[25], G. Herten[10], R.D. Heuer[25], J.C. Hill[5],
A. Hocker[9], K. Hoffman[8], R.J. Homer[1], A.K. Honma[8], D. Horváth[29,c], K.R. Hossain[28], R. Howard[27],
P. Hüntemeyer[25], P. Igo-Kemenes[11], K. Ishii[23], F.R. Jacob[20], A. Jawahery[17], H. Jeremie[18],
C.R. Jones[5], P. Jovanovic[1], T.R. Junk[6], N. Kanaya[23], J. Kanzaki[23], G. Karapetian[18], D. Karlen[6],
V. Kartvelishvili[16], K. Kawagoe[23], T. Kawamoto[23], R.K. Keeler[26], R.G. Kellogg[17], B.W. Kennedy[20],
D.H. Kim[19], K. Klein[11], A. Klier[24], S. Kluth[32], T. Kobayashi[23], M. Kobel[3], T.P. Kokott[3],
S. Komamiya[23], R.V. Kowalewski[26], T. Kress[4], P. Krieger[6], J. von Krogh[11], T. Kuhl[3], M. Kupper[24],
P. Kyberd[13], G.D. Lafferty[16], H. Landsman[21], D. Lanske[14], I. Lawson[26], J.G. Layter[4], A. Leins[31],
D. Lellouch[24], J. Letts[12], L. Levinson[24], R. Liebisch[11], J. Lillich[10], B. List[8], C. Littlewood[5],
A.W. Lloyd[1], S.L. Lloyd[13], F.K. Loebinger[16], G.D. Long[26], M.J. Losty[7], J. Lu[27], J. Ludwig[10],
A. Macchiolo[18], A. Macpherson[28,m], W. Mader[3], S. Marcellini[2], T.E. Marchant[16], A.J. Martin[13],
J.P. Martin[18], G. Martinez[17], T. Mashimo[23], P. Mättig[24], W.J. McDonald[28], J. McKenna[27],
T.J. McMahon[1], R.A. McPherson[26], F. Meijers[8], P. Mendez-Lorenzo[31], W. Menges[25], F.S. Merritt[9],
H. Mes[7], A. Michelini[2], S. Mihara[23], G. Mikenberg[24], D.J. Miller[15], W. Mohr[10], A. Montanari[2],
T. Mori[23], K. Nagai[8], I. Nakamura[23], H.A. Neal[12,f], R. Nisius[8], S.W. O'Neale[1], F.G. Oakham[7],
F. Odorici[2], H.O. Ogren[12], A. Oh[8], A. Okpara[11], M.J. Oreglia[9], S. Orito[23], G. Pásztor[8,j], J.R. Pater[16],
G.N. Patrick[20], J. Patt[10], P. Pfeifenschneider[14,i], J.E. Pilcher[9], J. Pinfold[28], D.E. Plane[8], B. Poli[2],
J. Polok[8], O. Pooth[8], M. Przybycień[8,d], A. Quadt[8], C. Rembser[8], P. Renkel[24], H. Rick[4], N. Rodning[28],
J.M. Roney[26], S. Rosati[3], K. Roscoe[16], A.M. Rossi[2], Y. Rozen[21], K. Runge[10], O. Runolfsson[8],
D.R. Rust[12], K. Sachs[6], T. Saeki[23], O. Sahr[31], E.K.G. Sarkisyan[22], C. Sbarra[26], A.D. Schaile[31],
O. Schaile[31], P. Scharff-Hansen[8], M. Schröder[8], M. Schumacher[25], C. Schwick[8], W.G. Scott[20],
R. Seuster[14,h], T.G. Shears[8,k], B.C. Shen[4], C.H. Shepherd-Themistocleous[5], P. Sherwood[15],
G.P. Siroli[2], A. Skuja[17], A.M. Smith[8], G.A. Snow[17], R. Sobie[26], S. Söldner-Rembold[10,e], S. Spagnolo[20],
M. Sproston[20], A. Stahl[3], K. Stephens[16], K. Stoll[10], D. Strom[19], R. Ströhmer[31], L. Stumpf[26],
B. Surrow[8], S.D. Talbot[1], S. Tarem[21], R.J. Taylor[15], R. Teuscher[9], M. Thiergen[10], J. Thomas[15],
M.A. Thomson[8], E. Torrence[9], S. Towers[6], D. Toya[23], T. Trefzger[31], I. Trigger[8], Z. Trócsányi[30,g],
E. Tsur[22], M.F. Turner-Watson[1], I. Ueda[23], B. Vachon[26], P. Vannerem[10], M. Verzocchi[8], H. Voss[8],
J. Vossebeld[8], D. Waller[6], C.P. Ward[5], D.R. Ward[5], P.M. Watkins[1], A.T. Watson[1], N.K. Watson[1],
P.S. Wells[8], T. Wengler[8], N. Wermes[3], D. Wetterling[11] J.S. White[6], G.W. Wilson[16], J.A. Wilson[1],
T.R. Wyatt[16], S. Yamashita[23], V. Zacek[18], D. Zer-Zion[8,l]

1

[1]School of Physics and Astronomy, University of Birmingham, Birmingham B15 2TT, UK

[2]Dipartimento di Fisica dell' Università di Bologna and INFN, I-40126 Bologna, Italy

[3]Physikalisches Institut, Universität Bonn, D-53115 Bonn, Germany

[4]Department of Physics, University of California, Riverside CA 92521, USA

[5]Cavendish Laboratory, Cambridge CB3 0HE, UK

[6]Ottawa-Carleton Institute for Physics, Department of Physics, Carleton University, Ottawa, Ontario K1S 5B6, Canada

[7]Centre for Research in Particle Physics, Carleton University, Ottawa, Ontario K1S 5B6, Canada

[8]CERN, European Organisation for Nuclear Research, CH-1211 Geneva 23, Switzerland

[9]Enrico Fermi Institute and Department of Physics, University of Chicago, Chicago IL 60637, USA

[10]Fakultät für Physik, Albert Ludwigs Universität, D-79104 Freiburg, Germany

[11]Physikalisches Institut, Universität Heidelberg, D-69120 Heidelberg, Germany

[12]Indiana University, Department of Physics, Swain Hall West 117, Bloomington IN 47405, USA

[13]Queen Mary and Westfield College, University of London, London E1 4NS, UK

[14]Technische Hochschule Aachen, III Physikalisches Institut, Sommerfeldstrasse 26-28, D-52056 Aachen, Germany

[15]University College London, London WC1E 6BT, UK

[16]Department of Physics, Schuster Laboratory, The University, Manchester M13 9PL, UK

[17]Department of Physics, University of Maryland, College Park, MD 20742, USA

[18]Laboratoire de Physique Nucléaire, Université de Montréal, Montréal, Quebec H3C 3J7, Canada

[19]University of Oregon, Department of Physics, Eugene OR 97403, USA

[20]CLRC Rutherford Appleton Laboratory, Chilton, Didcot, Oxfordshire OX11 0QX, UK

[21]Department of Physics, Technion-Israel Institute of Technology, Haifa 32000, Israel

[22]Department of Physics and Astronomy, Tel Aviv University, Tel Aviv 69978, Israel

[23]International Centre for Elementary Particle Physics and Department of Physics, University of Tokyo, Tokyo 113-0033, and Kobe University, Kobe 657-8501, Japan

[24]Particle Physics Department, Weizmann Institute of Science, Rehovot 76100, Israel

[25]Universität Hamburg/DESY, II Institut für Experimental Physik, Notkestrasse 85, D-22607 Hamburg, Germany

[26]University of Victoria, Department of Physics, P O Box 3055, Victoria BC V8W 3P6, Canada

[27]University of British Columbia, Department of Physics, Vancouver BC V6T 1Z1, Canada

[28]University of Alberta, Department of Physics, Edmonton AB T6G 2J1, Canada

[29]Research Institute for Particle and Nuclear Physics, H-1525 Budapest, P O Box 49, Hungary

[30]Institute of Nuclear Research, H-4001 Debrecen, P O Box 51, Hungary

[31]Ludwigs-Maximilians-Universität München, Sektion Physik, Am Coulombwall 1, D-85748 Garching, Germany

[32]Max-Planck-Institute für Physik, Föhring Ring 6, 80805 München, Germany

[a] and at TRIUMF, Vancouver, Canada V6T 2A3

[b] and Royal Society University Research Fellow

[c] and Institute of Nuclear Research, Debrecen, Hungary

[d] and University of Mining and Metallurgy, Cracow

[e] and Heisenberg Fellow

[f] now at Yale University, Dept of Physics, New Haven, USA

[g] and Department of Experimental Physics, Lajos Kossuth University, Debrecen, Hungary

[h] and MPI München

[i] now at MPI für Physik, 80805 München

[j] and Research Institute for Particle and Nuclear Physics, Budapest, Hungary

[k] now at University of Liverpool, Dept of Physics, Liverpool L69 3BX, UK

[l] and University of California, Riverside, High Energy Physics Group, CA 92521, USA

[m] and CERN, EP Div, 1211 Geneva 23.

# 1   Introduction

Since 1997 the LEP $e^+e^-$ collider has been operated at energies above the threshold for W-pair production. This offers a unique opportunity to study the hadronic decays of W bosons in a clean environment and to investigate the coupling strength of W bosons to different quark flavours. The fraction of W bosons decaying hadronically to different quark flavours is proportional to the sum of the squared magnitudes of the corresponding elements of the Cabibbo–Kobayashi–Maskawa (CKM) matrix [1]. A measurement of the production rates of different flavours therefore gives access to the individual CKM matrix elements.

In $e^+e^- \rightarrow W^+W^-$ events, the only heavy quark commonly produced is the charm quark. The production of bottom quarks is in fact highly suppressed due to the small magnitude of $|V_{ub}|$ and $|V_{cb}|$ and the large mass of the top quark, the weak partner of the bottom quark. This allows for a direct measurement of the production fraction of charm in W decays without a separation of charm and bottom quarks. The magnitude of the CKM matrix element $V_{cs}$ can then be derived from the charm production rate, using the knowledge of the other CKM matrix elements. So far direct measurements of $|V_{cs}|$ have limited precision compared to the other CKM matrix elements important in W decays, *i.e.* $|V_{ud}|$, $|V_{us}|$, and $|V_{cd}|$. The most recent evaluation of the magnitude of $V_{cs}$ from exclusive charm semielectronic decays yields $|V_{cs}| = 1.04 \pm 0.16$ [2].

In the analysis presented here, a value of the partial decay width $R_c^W \equiv \Gamma(W \rightarrow cX)/\Gamma(W \rightarrow \text{hadrons})$ is extracted from the properties of final state particles in W decays. Charm hadron identification is based upon jet properties, lifetime information, and semileptonic decay products in $W^+W^- \rightarrow q\overline{q}q\overline{q}$ and $W^+W^- \rightarrow q\overline{q}\ell\overline{\nu}_\ell$ events. The measured value of $R_c^W$ is then used to determine $|V_{cs}|$.

# 2   Data and Monte Carlo Samples

The data used for this analysis were recorded at LEP by the OPAL detector [3] at centre–of–mass energies around 183 GeV in 1997 and 189 GeV in 1998. OPAL[1] is a multipurpose high energy physics detector incorporating excellent charged and neutral particle detection and measurement capabilities. The integrated luminosities used for the analysis amount to $56.5\,\text{pb}^{-1}\,(180.2\,\text{pb}^{-1})$ at luminosity–weighted mean centre–of–mass energies of 182.7 GeV (188.6 GeV). In addition, $2.1\,\text{pb}^{-1}\,(3.1\,\text{pb}^{-1})$ of calibration data were collected at $\sqrt{s} \sim M_Z$ in 1997 (1998) and have been used for fine tuning of the Monte Carlo simulation.

To determine the selection criteria and tagging efficiencies, Monte Carlo samples were generated using the KORALW 1.42 [4] program, which utilizes JETSET 7.4 [5] for fragmentation, followed by a full simulation of the OPAL detector [6]. The centre–of–mass energies were set to $\sqrt{s} = 183\,\text{GeV}$ and 189 GeV with a W mass of $M_W = 80.33\,\text{GeV}$. Additional samples with different centre–of–mass energies and W masses were used to estimate the sensitivity to these parameters. Further samples generated with PYTHIA [7], HERWIG [8], and EXCALIBUR [9] were used to determine the model dependence of the measurement.

---

[1]The OPAL coordinate system is defined such that the $z$-axis is parallel to and in the direction of the $e^-$ beam, the $x$-axis lies in the plane of the accelerator pointing towards the centre of the LEP ring, and the $y$-axis is normal to the plane of the accelerator and has its positive direction defined to yield a right-handed coordinate system. The azimuthal angle, $\phi$, and the polar angle, $\theta$, are the conventional spherical coordinates.

|  | 183 GeV | | 189 GeV | |
|---|---|---|---|---|
| Type | $q\overline{q}\ell\nu$ | $q\overline{q}q\overline{q}$ | $q\overline{q}\ell\nu$ | $q\overline{q}q\overline{q}$ |
| Selected Events | 350 | 432 | 1235 | 1532 |
| $Z^0/\gamma \to q\overline{q}$ | $15.4 \pm 1.6$ | $77.4 \pm 8.5$ | $45.5 \pm 5.6$ | $240.0 \pm 15.9$ |
| $q\overline{q}q\overline{q}$ | $0.5 \pm 0.6$ | $12.4 \pm 2.8$ | $2.5 \pm 0.6$ | $70.3 \pm 12.3$ |
| $q\overline{q}\ell^+\ell^-$ | $10.2 \pm 1.2$ | $4.1 \pm 0.3$ | $27.6 \pm 2.7$ | $8.6 \pm 1.4$ |
| $We\overline{\nu}_e$ | $6.2 \pm 1.7$ | $0 \pm 1$ | $23.3 \pm 4.1$ | $0 \pm 1$ |
| Total Background | $32.4 \pm 2.7$ | $93.9 \pm 9.0$ | $98.9 \pm 7.5$ | $318.9 \pm 20.2$ |

Table 1: Number of selected WW candidate events and those expected from the main background sources for the selection at 183 GeV and 189 GeV. The "$q\overline{q}q\overline{q}$" background source refers to processes excluding doubly resonant W-pair production at tree level (CC03 diagrams). The entry labeled "$We\overline{\nu}_e$" refers to events where a singly produced W decays hadronically. The errors are the systematic errors on the background contributions, as evaluated in References [11, 12].

The dominant background sources for this analysis are $Z^0/\gamma \to q\overline{q}$ events and four–fermion final states which are not from $W^+W^-$ decays. Background samples were generated using the PYTHIA, HERWIG, EXCALIBUR, and GRC4F [10] generators. More details on the treatment of the backgrounds can be found in References [11, 12].

# 3 Event Selection

The WW event selections are the same as those used for the OPAL WW production cross–section measurements at $\sqrt{s} = 183\,\text{GeV}$ [11] and $189\,\text{GeV}$ [12]. Events not selected as $W^+W^- \to \ell^+\nu_\ell\ell'^-\overline{\nu}_{\ell'}$ candidates are passed to the $W^+W^- \to q\overline{q}\ell\nu_\ell$ selection procedure and may be classified as $q\overline{q}e\overline{\nu}_e$, $q\overline{q}\mu\overline{\nu}_\mu$, or $q\overline{q}\tau\overline{\nu}_\tau$ candidates. The $W^+W^- \to q\overline{q}q\overline{q}$ selection is applied to events that fail the preceding selections. It has been checked that the event selection introduces a negligible bias in the flavour composition. In this analysis, the small fraction of selected singly produced W bosons ($We\overline{\nu}_e$) which decay hadronically to a charm quark is considered as signal.

Since the identification of charm mesons relies heavily on lifetime and lepton information, the relevant parts of the detector were required to be operational while the data were recorded. Thus, in addition to the requirements which were already applied in References [11, 12], it was required that the silicon microvertex detector and the muon chambers were fully operational. After all cuts, a total of 350 (1235) $W^+W^- \to q\overline{q}\ell\nu_\ell$ candidates and 432 (1532) $W^+W^- \to q\overline{q}q\overline{q}$ candidates were selected at $183\,\text{GeV}$ ($189\,\text{GeV}$). A breakdown of the different background contributions is given in Table 1. The expected number of background events is calculated from the background cross–sections given in References [11, 12]; the errors correspond to the systematic errors quoted in these references.

# 4 Measurement of $R_c^W$

After the event selection, the hadronic part (which excludes the identified lepton) of a $q\overline{q}\ell\nu$ event is forced into two jets using the Durham algorithm [13], while $q\overline{q}q\overline{q}$ events are forced into four jets. Subsequently, a relative likelihood discriminant is calculated for each jet to separate jets originating from charm quarks and jets from u, d, and s quarks. This discriminant relies on jet and event shape properties, lifetime information, and lepton identification as described in the remaining parts of this

section. The resulting likelihood distribution is fitted to obtain the relative fractions of uds and charm jets.

In $q\overline{q}\ell\overline{\nu}_\ell$ events the two jets can be uniquely assigned to the decay of one W boson, while for $q\overline{q}q\overline{q}$ events the four jets have to be grouped into pairs that are assumed to originate from the decay of one W boson. The jet pairing is chosen using a kinematic fit to find the jet combination which is most compatible with the production of two on-shell W bosons with a mass of 80.33 GeV. After the jet pairing has been performed in $q\overline{q}\ell\overline{\nu}_\ell$ and $q\overline{q}q\overline{q}$ events, the jet energies are calculated in a kinematic fit, imposing energy–momentum conservation and equality of the masses of both W candidates. If the kinematic fit fails, the jet energies of each jet pair are scaled so that their sum equals the beam energy. The choice of the jet pairing influences the result of the present analysis only through the values of the jet angle $\theta_{\mathrm{jet}}$ in the di-jet rest frame and the di-jet angle $\theta_{\mathrm{W}}$ in the laboratory frame, both of which are calculated from the jet momenta determined by the kinematic fit. These two angles are employed in the likelihood functions as described in Sections 4.2 and 4.3. It has been checked in the W mass measurement analysis [14, 15] and in an analysis concerned with properties of hadronically decaying W bosons [16] that jet properties relevant for the jet pairing algorithm and the kinematic fit are well modelled in the Monte Carlo simulation.

## 4.1   Secondary Vertex Tag

Weakly decaying charm hadrons have lifetimes between 0.2 ps and 1 ps [2], leading to typical decay lengths of a few hundred microns to a few millimetres at LEP2 energies. These relatively long–lived particles produce secondary decay vertices which are significantly displaced from the primary event vertex. The primary vertex in an event is found by fitting all charged tracks to a common point in space [17]. Its determination is improved by using the average beam position as a constraint with RMS values of 150 $\mu$m in $x$, dominated by the width of the beam, about 20 $\mu$m in $y$, and less than 1 cm in $z$.

In the search for charm decay products, tracks in the central detector and clusters in the electro-magnetic calorimeter within a given jet are considered. Tracks used to find secondary vertices must fulfill the quality criteria used in the WW cross-section analyses [11, 12]. Additionally, the tracks are required to have a momentum larger than 0.75 GeV, a signed distance of closest approach to the primary vertex in the $r\phi$ plane (2D-impact parameter) 0 cm $< d_0 < 0.3$ cm, and an error on the impact parameter, $\sigma_{d_0}$, smaller than 0.1 cm. From the tracks which fulfill these criteria, the tracks which are most likely to originate from the decay products of a charm hadron are identified via an iterative procedure. Particles from charm hadron decays tend to have a large momentum and a large rapidity $y = \frac{1}{2}\ln\left(\frac{E+p_\parallel}{E-p_\parallel}\right)$ (where $p_\parallel$ is the particle's momentum component parallel to the jet direction and $E$ is its energy) compared to fragmentation tracks, and their combined invariant mass should be compatible with a charm hadron mass. Therefore for each track and electromagnetic cluster which is not associated to any track, the rapidity $y$ is calculated assuming the charged pion mass for tracks and zero mass for unassociated clusters. The track or cluster with the lowest rapidity is removed from the sample and the invariant mass of the remaining tracks and clusters is calculated. This procedure is repeated until the mass of the remaining group of tracks and clusters falls below 2.5 GeV. This procedure selects preferentially tracks from the decay of charm hadrons [18].

All selected tracks in the jet are fitted to a common vertex in three dimensions. Tracks which contribute more than 4 to the $\chi^2$ of this fit are removed and the fit is repeated. The procedure is stopped when all tracks pass the $\chi^2$ requirement. At least two tracks are required to remain in the fit for the secondary vertex finding to be successful. Once tracks are associated to a secondary vertex, the

5

distance $L$ between the primary and the secondary vertex and its error $\sigma_L$ are computed. The decay length significance of a secondary vertex, $L/\sigma_L$, is required to be positive (*i.e.* $L/\sigma_L > 0$), where $L$ is given a positive sign if the secondary vertex is displaced from the primary vertex along the direction of the jet momentum.

Jets containing a good secondary vertex are then used to tag charm decay products by means of an artificial neural network (ANN) [19] to enhance the charm purity at a given efficiency. The nine ANN input variables are: the decay length significance $L/\sigma_L$ of the secondary vertex; the primary vertex joint probability (for a definition, see Reference [20]); $E_{\mathrm{vertex}}/E_{\mathrm{beam}}$, where $E_{\mathrm{vertex}}$ is the sum of the energy of all the tracks assigned to the secondary vertex and $E_{\mathrm{beam}}$ is the beam energy; the distance of closest approach to the primary event vertex in $r\phi z$ (3D) of the pseudo–particle formed from all the tracks in the secondary vertex; the normalised weighted average (weighted by the measured error) of all the track 2D-impact parameters within the secondary vertex; the highest momentum of the charged particles in the secondary vertex; the invariant mass of the vertex; the largest track 3D-impact parameter in the secondary vertex; and the second largest track 3D-impact parameter in the secondary vertex.

The same vertex ANN is used for $W^+W^- \to q\overline{q}q\overline{q}$ and $W^+W^- \to q\overline{q}\ell\overline{\nu}_\ell$ events. The distributions of the two most discriminating input variables for the vertex ANN are shown in Figure 1. Typically, charm hadrons have secondary vertices which are displaced from the primary vertex and charged tracks associated with charm particles have a lower probability to come from the primary vertex. Figure 2a shows a comparison of the ANN output between data and Monte Carlo for $\sqrt{s} = 183 - 189\,\mathrm{GeV}$. The simulation of the OPAL tracking detectors [6] requires a detailed understanding of the track-finding efficiency and resolution. This is achieved by tuning the Monte Carlo simulation with the calibration data taken at the $Z^0$ resonance. Figure 3a shows the distribution of $L/\sigma_L$ for secondary vertices. The effect of a $5\,\%$ variation of the tracking resolution used to assess the systematic uncertainty is also depicted.

## 4.2   Lepton Tag

About $20\,\%$ of all charm hadrons decay semileptonically and produce an electron or a muon in the final state. Because of the relatively large mass and hard fragmentation of the charm quark compared to light quarks, this lepton is expected to have a larger momentum than leptons from other sources (except the small contribution from semileptonic bottom decays in background events). Therefore, identified electrons and muons can be used as tags for charm hadrons in W boson decays.

In a first step, the leptons are identified using ANN algorithms. The electron ANN described in References [21, 22] is used. Its most important input variables are the specific ionization in the central jet chamber $(\mathrm{d}E/\mathrm{d}x)$ of the electron candidate track and the ratio of the associated energy deposited in the electromagnetic calorimeter to the momentum of this track $(E/p)$. Photon conversions are rejected from the sample using another dedicated ANN [21, 22]. The muon ANN [23] is based on information from the tracking detectors (including $\mathrm{d}E/\mathrm{d}x$), the hadronic calorimeter, and the muon chambers. The lepton candidates have to be well contained in the detector ($|\cos\theta_\ell| < 0.9$, where $\theta_\ell$ is the polar angle with respect to the $e^-$ beam direction) and are required to have momentum $p_\ell > 2\,\mathrm{GeV}$.

The most energetic lepton candidate in each jet is used to calculate a relative likelihood discriminant with the goal of separating leptons in charm decays from leptons from other sources. Dedicated likelihood functions are set up for electrons and muons in $W^+W^- \to q\overline{q}q\overline{q}$ and $W^+W^- \to q\overline{q}\ell\overline{\nu}_\ell$ events, using additional variables that describe properties of the lepton within a jet and enhance the

6

| Tagging | 183 GeV | | 189 GeV | |
|---|---|---|---|---|
| Efficiency (%) | $q\overline{q}\ell\overline{\nu}$ | $q\overline{q}q\overline{q}$ | $q\overline{q}\ell\overline{\nu}$ | $q\overline{q}q\overline{q}$ |
| $\epsilon_{W\to u}$ | $4.3 \pm 0.5$ | $3.8 \pm 0.3$ | $4.9 \pm 0.5$ | $4.4 \pm 0.3$ |
| $\epsilon_{W\to d}$ | $3.1 \pm 0.4$ | $3.0 \pm 0.2$ | $3.2 \pm 0.4$ | $3.1 \pm 0.2$ |
| $\epsilon_{W\to s}$ | $3.2 \pm 0.4$ | $3.0 \pm 0.2$ | $3.3 \pm 0.4$ | $3.1 \pm 0.2$ |
| $\epsilon_{W\to c}$ | $18.1 \pm 0.6$ | $15.8 \pm 0.4$ | $18.9 \pm 0.6$ | $16.7 \pm 0.4$ |
| $\epsilon_{bgd}$ | $6.0 \pm 2.7$ | $4.7 \pm 1.0$ | $8.0 \pm 2.1$ | $5.4 \pm 0.8$ |

Table 2: Tagging efficiencies (in %) after the WW selection from Monte Carlo simulation for u, d, s, and c jets in WW events and for jets from background events, for a cut on the combined likelihood of 0.7. The values are shown separately for events at 183 GeV and 189 GeV and for $q\overline{q}\ell\overline{\nu}$ and $q\overline{q}q\overline{q}$ events. The errors are statistical only.

separation of charm jets from uds jets. The likelihood calculation is done using the method described in Reference [24]. The following input variables are used both for electrons and for muons: the output of the electron or muon ANN; the magnitude of the cosine of the polar angle of the lepton candidate $|\cos\theta_\ell|$; and the magnitude of the momentum of the lepton candidate $p_\ell$.

In $q\overline{q}q\overline{q}$ events, where the charge of the decaying W boson is not known, the likelihood function also uses the product of the lepton charge and the cosine of the W production angle, $Q_\ell \cos\theta_W$, where $\theta_W$ is defined as the polar angle of the sum of momenta of both jets of the pair that contains the lepton. This quantity makes use of the strong forward–backward asymmetry of the produced W bosons.

In $q\overline{q}\ell\overline{\nu}$ events, where the charge of the W boson decaying leptonically is known, the likelihood function uses the product of the charge of the lepton tagged in the charm decay and the charge of the lepton from the leptonically decaying W. Finally, for electron candidates, the likelihood discriminant employs the output of the conversion finder ANN to suppress electrons from photon conversions.

In Figure 2b the likelihood output of the lepton tag is shown for data and Monte Carlo at $\sqrt{s} = 183 - 189$ GeV. In this analysis precise modelling of the lepton identification is important. The lepton reconstruction efficiencies in the Monte Carlo simulation were tuned to match the values obtained from data collected at the $Z^0$ resonance. Figures 3b-c show the $E/p$ and normalised $dE/dx$ distributions of electron candidates. Reasonable agreement between data and Monte Carlo simulation is observed. The variables used for muon identification are also well described in the simulation.

## 4.3   Combined Tag

For each jet, the vertex ANN and the lepton likelihood discriminant are merged into a single quantity by an additional likelihood function. This combined likelihood discriminant uses two additional variables: the cosine of the jet angle $\cos\theta_{jet}$ in the rest frame of the W boson with respect to the W momentum direction and the likelihood output of the WW event selection [11, 12]. The jet angle in the di-jet rest frame helps to separate jets originating from up–type and down–type quarks. Due to the polarisation of the W bosons and the $V - A$ nature of the weak interaction, up–type quarks tend to be produced preferentially in the backward direction with respect to the W flight direction, while down–type quarks are found more often in the forward direction. The likelihood output of the WW event selection suppresses false tags from background events, especially from $Z^0/\gamma \to b\overline{b}$ events.

In Figure 4a the combined likelihood output is shown, illustrating the discriminating power between charm and light flavoured jets. The efficiency and purity for a particular cut on the combined likelihood

output are also depicted in Figure 4b. Table 2 lists the tagging efficiencies for jets in WW and background events that result from a cut on the likelihood output at the optimal value of 0.7. The tagging efficiencies at 189 GeV are slightly higher due to the extra boost of the W bosons. These values are not directly used to derive $R_c^W$, but are quoted to give an impression of the performance of the charm tag.

## 4.4 Determination of $R_c^W$

To extract $R_c^W$ from the data, a binned maximum likelihood fit is performed to the combined likelihood distributions. Template histograms for the charm, light–flavoured, and non–WW background components are produced from the main Monte Carlo samples. They are referred to as the probability density functions (pdf) for the various components. Using this fitting method improves the statistical sensitivity of the measurement compared to simply counting the number of jets that pass a cut on the likelihood output. The function used to fit the data (see Figure 4a) is:

$$ -\ln \mathcal{L} \;=\; -\sum_{i=1}^{N} n_i \, \ln \left\{ (1 - F_{\rm bkg}) \left( \tfrac{1}{2} R_c^W \, \mathcal{P}_c^i + [1 - \tfrac{1}{2} R_c^W] \, \mathcal{P}_{\rm uds}^i \right) + F_{\rm bkg} \, \mathcal{P}_{\rm bkg}^i \right\}, \tag{1} $$

with

$i$: Bin index in the combined likelihood distribution;

$n_i$: Number of jets in the $i^{\rm th}$ bin;

$N$: Number of bins in the combined likelihood distribution;

$\mathcal{P}_c^i$: Probability for a charm jet to appear in the $i^{\rm th}$ bin (W $\to$ c X pdf);

$\mathcal{P}_{\rm uds}^i$: Probability for a uds jet to appear in the $i^{\rm th}$ bin (W $\to$ light flavour pdf);

$F_{\rm bkg}$: Fraction of background jets;

$\mathcal{P}_{\rm bkg}^i$: Probability for a non–WW jet to appear in the $i^{\rm th}$ bin (non–WW background pdf).

The result of the fit for $R_c^W$ is:

$$ R_c^W = 0.493 \pm 0.090 \quad \text{at 183 GeV} $$

and

$$ R_c^W = 0.478 \pm 0.047 \quad \text{at 189 GeV}. $$

where the errors are statistical only. The $\chi^2$/(degree of freedom) of the fits are 17.2/24 at 183 GeV and 35.4/24 at 189 GeV.

## 4.5 Systematic uncertainties

Since the reference histograms, the efficiencies, and the background for the calculation of $R_c^W$ were taken from a Monte Carlo simulation, the analysis depends on the proper modelling of the data distributions in the simulation. The sources of systematic error are listed in Table 3 and are discussed below. Unless otherwise noted, all changes were applied to signal and background Monte Carlo samples.

8

- *Hadronisation model:* The Pythia Monte Carlo sample, which uses the Lund string fragmentation as implemented in Jetset [5], was compared to a sample generated with Herwig [8], which uses cluster fragmentation. The samples differ in their parton showering and hadronisation.

- W *mass and centre–of–mass energy:* As the jet pairing depends on the W mass, $M_W$, and the centre–of–mass energy, $\sqrt{s}$, the analysis was repeated with different W masses and at different centre–of–mass energies. The W mass was varied by $100\,\mathrm{MeV}$, which covers both the experimental uncertainty and the differences between the current world average mass [2] and the value used in the Monte Carlo. The centre–of–mass energy was varied by the difference between the luminosity–weighted centre–of–mass energies in data and the value of $\sqrt{s}$ used in the main Monte Carlo samples.

- *Charm fragmentation:* At $\sqrt{s} = M_Z$, the mean scaled energy of weakly decaying charm hadrons was found to be $\langle x_D(M_Z)\rangle = 0.484 \pm 0.008$ [25]. No measurements of this quantity exist for W decays, but it is expected to be similar to that in Z decays. The changes in the charm fragmentation due to QCD effects were taken from Jetset [5]. To assess the systematic uncertainty, $\langle x_D(M_W)\rangle$ was varied by the experimental uncertainty obtained on $\langle x_D(M_Z)\rangle$, *i.e.* 0.008. The fragmentation schemes of Peterson [26], Collins and Spiller [27], Kartvelishvili [28] and the Lund group [29] were used to assess a possible discrepancy on the shape of the fragmentation function. The largest variation was assigned as the systematic error.

- *Background cross–section:* In the fit for extracting $R_c^W$, the fraction of background was varied according to the error on the expected fraction of background events from References [11, 12].

- *Background composition:* The various background sources have different probabilities to fake a charm jet. The background composition was varied within the uncertainties given in Table 1.

- *Charm hadron fractions:* The fractions of the weakly decaying charm hadrons were varied within their experimental errors according to Reference [25].

- *Light quark composition:* The shape of the reference histogram for light–flavoured quarks depends on the relative fractions of the u, d, and s jets. The quark flavour fractions were varied according to the actual errors on the CKM matrix [2] so that the error covers the effect of assumptions concerning the CKM matrix elements on the uds template histogram. The number of bottom hadrons from W bosons was also doubled to ensure that the measured $R_c^W$ was insensitive to the bottom fraction in W decays.

- *Vertex reconstruction:* The correct modelling of the detector resolution in the Monte Carlo simulation is of paramount importance for the description of the probability to find a secondary vertex. This was checked by comparing the track parameters between calibration data collected at $\sqrt{s} \sim M_Z$ and Monte Carlo simulation. The sensitivity to the vertex reconstruction was assessed by degrading or improving the tracking resolution in the Monte Carlo. It was found that changing the track parameters resolution by $\pm 5\%$ covers the range of the observed differences between data and Monte Carlo (see Figure 3a) in the vertex ANN input and output distributions.

- *Charm hadron lifetimes:* The lifetimes of the weakly decaying charm hadrons were varied within their experimental errors according to Reference [2].

- *Charm decay multiplicity:* The performance of the secondary vertex finder depends on the multiplicity of the final state of the charm hadrons. The relative abundance of 1, 2, 3, 4, 5, and 6 prong charm decays was changed in the Monte Carlo within their experimental errors [30]. Similarly, the relative abundance of neutral pions was varied in the Monte Carlo within the experimental errors [30].

| Source of Systematic Error | $\Delta R_{\mathrm{c}}^{\mathrm{W}}$ | |
|---|---|---|
| | 183 GeV | 189 GeV |
| Hadronisation Model | 0.011 | 0.012 |
| Centre–of–mass Energy | 0.007 | 0.005 |
| Mass of the W Boson | 0.004 | 0.003 |
| Charm Fragmentation Function | 0.007 | 0.007 |
| Background Cross-Section | 0.006 | 0.005 |
| Background Composition | 0.010 | 0.009 |
| Charm Hadron Fractions | 0.006 | 0.007 |
| Light Quark Composition | 0.007 | 0.005 |
| Vertex Reconstruction | 0.016 | 0.017 |
| Charm Hadron Lifetimes | 0.003 | 0.002 |
| Charm Decay Multiplicity | 0.010 | 0.010 |
| Lepton Identification | 0.012 | 0.014 |
| Lepton Energy Spectrum | 0.003 | 0.003 |
| Branching ratio Br(c $\rightarrow \ell$) | 0.006 | 0.006 |
| Total systematic error | 0.032 | 0.032 |
| Statistical error | 0.090 | 0.047 |
| Value of $R_{\mathrm{c}}^{\mathrm{W}}$ | 0.493 | 0.478 |

Table 3: Summary of the experimental systematic errors, statistical errors, and central values from the binned maximum likelihood fit on $R_{\mathrm{c}}^{\mathrm{W}}$ at 183 GeV and 189 GeV.

- *Lepton identification:* The modelling of the input variables of the ANN for electron identification has been intensively studied at LEP1 [22], while the performance of the muon tagging ANN has been investigated using various control samples of calibration data collected at the $\mathrm{Z}^0$ resonance during each year of LEP2 [23]. The relative error of the efficiency to identify a genuine electron (muon) has been estimated to be 4 % (3 %), and the relative error on the probability to wrongly identify a hadron as a lepton has been evaluated to be around 16 % (10 %) for electrons (muons) [22, 23]. By studying the $\mathrm{d}E/\mathrm{d}x$ distributions for electron candidates in calibration data taken at the $\mathrm{Z}^0$ mass in 1997 and 1998, it was found that a shift of the mean $\mathrm{d}E/\mathrm{d}x$ of 0.04 keV/cm (0.3%) and a scaling by 1% of the $\mathrm{d}E/\mathrm{d}x$ resolution in data was needed to correct a slight discrepancy between Monte Carlo and data. This effect was also taken into account in the assignment of the uncertainty on the electron tagging efficiency. The (mis)identification probabilities for electrons and muons were varied by reweighting the Monte Carlo events and the largest resulting change in $R_{\mathrm{c}}^{\mathrm{W}}$ was taken as the systematic error. It was verified that the variation of efficiencies and $\mathrm{d}E/\mathrm{d}x$ resolution was sufficient to describe the possible differences between data and Monte Carlo (see Figures 3b-c).

- *Lepton energy spectrum from semileptonic charm decays:* The energy spectrum of the lepton in the rest frame of the weakly decaying charm hadron was reweighted from the spectrum implemented in JETSET to the ISGW [31] and ACCMM [32] models; the parameters $p_{\mathrm{f}}$ and $m_{\mathrm{s}}$ of the ACCMM model were varied in the range recommended in Reference [25].

- *Branching ratio* Br(c $\rightarrow \ell$): The branching fraction for inclusive charm decays to leptons was varied within the range Br(c $\rightarrow \ell$) = 0.098 $\pm$ 0.005 [25] by reweighting the Monte Carlo events.

The size of the systematic errors is very similar for the samples at 183 GeV and 189 GeV. The dominant systematic errors are those associated with the vertex reconstruction and lepton identification.

10

| CKM matrix element | Value |
|:---:|:---:|
| $\lvert V_{\mathrm{ud}}\rvert$ | $0.9735 \pm 0.0008$ |
| $\lvert V_{\mathrm{us}}\rvert$ | $0.2196 \pm 0.0023$ |
| $\lvert V_{\mathrm{ub}}\rvert/\lvert V_{\mathrm{cb}}\rvert$ | $0.090 \ \pm 0.025$ |
| $\lvert V_{\mathrm{cd}}\rvert$ | $0.224 \ \pm 0.016$ |
| $\lvert V_{\mathrm{cb}}\rvert$ | $0.0402 \pm 0.0019$ |

Table 4: Values of the CKM matrix elements used in the calculation of $\lvert V_{\mathrm{cs}}\rvert$ from $R_{\mathrm{c}}^{\mathrm{W}}$. The values are taken from Reference [2].

## 5 Results

The result of the charm tag analysis is

$$R_{\mathrm{c}}^{\mathrm{W}} = 0.493 \pm 0.090 \,(\text{stat.}) \pm 0.032 \,(\text{syst.}) \quad \text{at 183 GeV}$$

and

$$R_{\mathrm{c}}^{\mathrm{W}} = 0.478 \pm 0.047 \,(\text{stat.}) \pm 0.032 \,(\text{syst.}) \quad \text{at 189 GeV.}$$

The combined value of $R_{\mathrm{c}}^{\mathrm{W}}$ obtained at $\sqrt{s} = 183\,\mathrm{GeV}$ and $189\,\mathrm{GeV}$ is

$$R_{\mathrm{c}}^{\mathrm{W}} = 0.481 \pm 0.042 \,(\text{stat.}) \pm 0.032 \,(\text{syst.}),$$

where the systematic uncertainties are treated as being fully correlated.

## 6 Extraction of $\lvert V_{\mathrm{cs}}\rvert$

It is possible to extract $\lvert V_{\mathrm{cs}}\rvert$ from $R_{\mathrm{c}}^{\mathrm{W}}$ using the relation

$$R_{\mathrm{c}}^{\mathrm{W}} = \frac{\lvert V_{\mathrm{cd}}\rvert^2 + \lvert V_{\mathrm{cs}}\rvert^2 + \lvert V_{\mathrm{cb}}\rvert^2}{\lvert V_{\mathrm{ud}}\rvert^2 + \lvert V_{\mathrm{us}}\rvert^2 + \lvert V_{\mathrm{ub}}\rvert^2 + \lvert V_{\mathrm{cd}}\rvert^2 + \lvert V_{\mathrm{cs}}\rvert^2 + \lvert V_{\mathrm{cb}}\rvert^2}, \tag{2}$$

which leads to

$$\lvert V_{\mathrm{cs}}\rvert = \sqrt{\frac{R_{\mathrm{c}}^{\mathrm{W}}}{1 - R_{\mathrm{c}}^{\mathrm{W}}}\left(\lvert V_{\mathrm{ud}}\rvert^2 + \lvert V_{\mathrm{us}}\rvert^2 + \lvert V_{\mathrm{ub}}\rvert^2\right) - \lvert V_{\mathrm{cd}}\rvert^2 - \lvert V_{\mathrm{cb}}\rvert^2}. \tag{3}$$

Using the values of the other CKM matrix elements listed in Table 4, one gets

$$\lvert V_{\mathrm{cs}}\rvert = 0.93 \pm 0.08 \,(\text{stat.}) \pm 0.06 \,(\text{syst.}) \pm 0.004 \,(\text{CKM}),$$

where the last error is due to the uncertainty on the CKM matrix elements used in the calculation.

A more precise value for $\lvert V_{\mathrm{cs}}\rvert$ can be obtained based on the Standard Model prediction of the decay width of the W boson to final states containing charm quarks:

$$\Gamma\left(\mathrm{W} \to \mathrm{c}\,\mathrm{X}\right) = \frac{C G_{\mathrm{F}} M_{\mathrm{W}}^3}{6\sqrt{2}\pi}\left(\lvert V_{\mathrm{cd}}\rvert^2 + \lvert V_{\mathrm{cs}}\rvert^2 + \lvert V_{\mathrm{cb}}\rvert^2\right), \tag{4}$$

with $\frac{C G_{\mathrm{F}} M_{\mathrm{W}}^3}{6\sqrt{2}\pi} = (705 \pm 4)\,\mathrm{MeV}$ [2] and the color factor $C$ given by [2]

$$C = 3\left(1 + \frac{\alpha_{\mathrm{s}}\left(M_{\mathrm{W}}\right)}{\pi} + 1.409\frac{\alpha_{\mathrm{s}}^2\left(M_{\mathrm{W}}\right)}{\pi^2} - 12.77\frac{\alpha_{\mathrm{s}}^3\left(M_{\mathrm{W}}\right)}{\pi^3}\right). \tag{5}$$

$\Gamma(W \to cX)$ can be evaluated from $R_c^W$ using the relation

$$\Gamma(W \to cX) = R_c^W \, Br(W \to hadrons) \, \Gamma_{tot}^W. \qquad (6)$$

Using the PDG values $Br(W \to hadrons) = 0.6848 \pm 0.0059$ and[2] $\Gamma_{tot}^W = (2.12 \pm 0.05)\,GeV$ [2] together with the measurement of $R_c^W$ presented in this letter, one gets

$$\Gamma(W \to cX) = [698 \pm 61\,(stat.) \pm 46\,(syst.) \pm 18\,(ext.)]\,MeV,$$

where the last error is due to the uncertainties on the external parameters $\Gamma_{tot}^W$ and $Br(W \to hadrons)$. This corresponds to

$$|V_{cd}|^2 + |V_{cs}|^2 + |V_{cb}|^2 = 0.990 \pm 0.087\,(stat.) \pm 0.065\,(syst.) \pm 0.026\,(ext.).$$

Subtracting the off–diagonal CKM matrix elements, using the values listed in Table 4, results in

$$|V_{cs}| = 0.969 \pm 0.045\,(stat.) \pm 0.034\,(syst.) \pm 0.013\,(ext.) \pm 0.004\,(CKM),$$

where the last error is due to the uncertainties on the CKM matrix elements used in the calculation. The determination of $|V_{cs}|$ from Equations (4) and (6) only involves the CKM matrix elements for the transition $W \to cX$ and well measured parameters such as $\Gamma_{tot}^W$ and $Br(W \to hadrons)$. It is therefore more precise than the method which relies on Equation (3). Both results of $|V_{cs}|$ presented here are compatible with the direct determination from $D$ semielectronic decays which yields $|V_{cs}| = 1.04 \pm 0.16$ [2].

# 7    Summary

Using data taken with the OPAL detector at LEP at centre–of–mass energies of $183\,GeV$ and $189\,GeV$, the ratio $R_c^W = \Gamma(W \to cX)/\Gamma(W \to hadrons)$ has been measured using a technique based on jet properties, lifetime information, and leptons from charm decays. The combined result is

$$R_c^W = 0.481 \pm 0.042\,(stat.) \pm 0.032\,(syst.),$$

in agreement with the Standard Model expectation of 0.5. This result is consistent with the Standard Model prediction that the W boson couples to up and charm quarks with equal strength and it is in agreement with the recent measurements of DELPHI [34] and ALEPH [35].

Using the results from direct measurements of the other CKM matrix elements, $|V_{cs}|$ can be calculated from $R_c^W$, yielding $|V_{cs}| = 0.93 \pm 0.10$. A more precise value for $|V_{cs}|$ can be derived from the measurements of $R_c^W$, $Br(W \to hadrons)$, and $\Gamma_{tot}^W$:

$$|V_{cs}| = 0.969 \pm 0.058.$$

This can be compared to a more indirect determination of $|V_{cs}|$ by OPAL from the ratio of the W decay widths to $q\overline{q}$ and $\ell\overline{\nu}_\ell$, which yields $|V_{cs}| = 1.014 \pm 0.029\,(stat.) \pm 0.014\,(syst.)$ [12] under the assumption that the W boson couples with equal strength to quarks and leptons. It should be noted that the ratio $Br(W \to q\overline{q})/Br(W \to \ell\overline{\nu}_\ell)$ is not used in the analysis presented here, so that these are independent determinations of $|V_{cs}|$.

---

[2]The most precise measurements of $\Gamma_{tot}^W$ are determined from the quantity $\mathcal{R} = \frac{\sigma(p\overline{p} \to W+X) \cdot Br(W \to e\overline{\nu})}{\sigma(p\overline{p} \to Z^0+X) \cdot Br(Z^0 \to e^+e^-)}$. In [33], the coupling of the W boson to light quarks is needed as input; however, direct measurements of the corresponding CKM matrix elements are so precise that it introduces a negligible uncertainty on $\Gamma_{tot}^W$.

# Acknowledgements

# References

[1] N. Cabibbo, Phys. Rev. Lett. **10** (1963) 531;
M. Kobayashi and T. Maskawa, Prog. Theor. Phys. **49** (1973) 652.

[2] D.E.. Groom *et al.*, Eur. Phys. J. **C15** (2000) 1.

[3] OPAL Collaboration, K. Ahmet *et al.*, Nucl. Instr. Meth. **A305** (1991) 275;
P.P. Allport *et al.*, Nucl. Instr. Meth. **A324** (1993) 34;
P.P. Allport *et al.*, Nucl. Instr. Meth. **A346** (1994) 476;
S. Anderson *et al.*, Nucl. Instr. Meth. **A403** (1998) 326.

[4] M. Skrzypek *et al.*, Comput. Phys. Commun. **94** (1996) 216;
M. Skrzypek *et al.*, Phys. Lett. **B372** (1996) 289.

[5] T. Sjöstrand, Comput. Phys. Commun. **39** (1986) 347;
T. Sjöstrand and H.–U. Bengtsson, Comput. Phys. Commun. **43** (1987) 367.

[6] J. Allison *et al.*, Nucl. Instr. Meth. **A317** (1992) 47.

[7] T. Sjöstrand, Comput. Phys. Commun. **82** (1994) 74.

[8] G. Marchesini *et al.*, Comput. Phys. Commun. **67** (1992) 465.

[9] F.A. Berends, R. Pittau and R. Kleiss, Comput. Phys. Commun. **85** (1995) 437.

[10] J. Fujimoto *et al.*, Comput. Phys. Commun. **100** (1997) 128.

[11] OPAL Collaboration, G. Abbiendi *et al.*, Eur. Phys. J. **C8** (1999) 191.

[12] OPAL Collaboration, W$^+$W$^-$ *Production Cross Section and* W *Branching Fractions in* e$^+$e$^-$ *Collisions at 189* GeV, OPAL PR321, CERN-EP-2000-101 (2000), Submitted to Phys. Lett. B.

[13] S. Catani *et al.*, Phys. Lett. **B269** (1991) 432.

[14] OPAL Collaboration, G. Abbiendi *et al.*, Phys. Lett. **B453** (1999) 138.

[15] OPAL Collaboration, *Measurement of the Mass and Width of the* W *Boson in* e$^+$e$^-$ *Collisions at 189,*GeV, OPAL PR320, CERN-EP-2000-099 (2000), Submitted to Phys. Lett. B.

[16] OPAL Collaboration, G. Abbiendi *et al.*, Phys. Lett. **B453** (1999) 153.

[17] OPAL Collaboration, K. Ackerstaff *et al.*, Z. Phys. **C74** (1997) 1.

[18] OPAL Collaboration, K. Ackerstaff *et al.*, Eur. Phys. J. **C1** (1998) 439.

[19] C. Peterson, T. Rögnvaldsson and L. Lönnblad, *JETNET 3.0 - A Versatile Artificial Neural Network Package,* LU–TP–93–29, CERN–TH.7135/94.

[20] ALEPH Collaboration, D. Buskulic *et al.*, Phys. Lett. **B313** (1993) 535.

[21] OPAL Collaboration, G. Alexander *et al.*, Z. Phys. **C70** (1996) 357.

[22] OPAL Collaboration, G. Abbiendi *et al.*, Eur. Phys. J. **C8** (1999) 217.

[23] OPAL Collaboration, *Measurements of $R_{\rm b}$, $A_{\rm FB}^{\rm b}$, and $A_{\rm FB}^{\rm c}$ in* e$^+$e$^-$ *Collisions at 130–189* GeV, CERN-EP/99-170 (1999), Submitted to Eur. Phys. J. C.

[24] D. Karlen, Comp. in Phys. **12:4** (1998) 380.

[25] ALEPH, DELPHI, L3, and OPAL Collaborations: Nucl. Instr. Meth. **A378** (1996) 101; Updates of the recommendations are given in the LEP electroweak working group: *Input Parameters for the LEP Electroweak Heavy Flavour Results for Summer 1998 Conferences*, internal note LEPHF/98–01 (URL: `http://www.cern.ch/LEPEWWG/heavy/`).

[26] C. Peterson, D. Schlatter, I. Schmitt, and P.M. Zerwas, Phys. Rev. **D27** (1983) 105.

[27] P. Collins and T. Spiller, J. Phys. **G11** (1985) 1289.

[28] V.G. Kartvelishvili, A.K. Likhoded and V.A. Petrov, Phys. Lett. **B78** (1978) 615.

[29] B. Anderson, G. Gustafson and B. Söderberg, Z. Phys. **C20** (1983) 317.

[30] Mark III Collaboration, D. Coffman *et al.*, Phys. Lett. **B263** (1991) 135.

[31] N. Isgur, D. Scora, B. Grinstein, M.B. Wise, Phys. Rev. **D39** (1989) 799; N. Isgur and M.B. Wise, Phys. Rev. **D41** (1990) 151.

[32] G. Altarelli *et al.*, Nucl. Phys. **B208** (1982) 365.

[33] D0 Collaboration, S. Abachi *et al.*, Phys. Rev. Lett. **75** (1995) 1456; CDF Collaboration, F. Abe *et al.*, Phys. Rev. **D52** (1995) 2624.

[34] DELPHI Collaboration, P. Abreu *et al.*, Phys. Lett. **B439** (1998) 209.

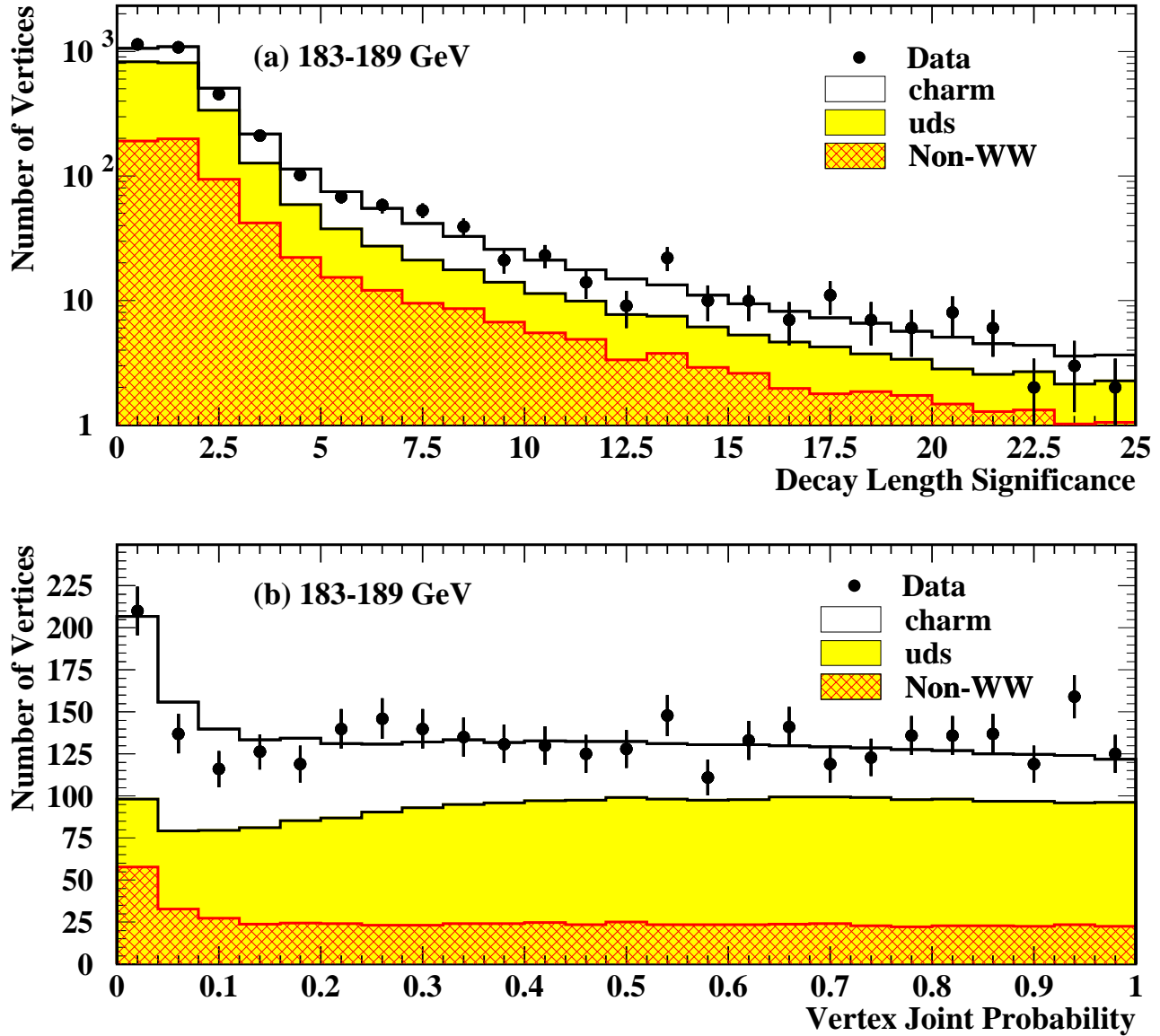[35] ALEPH Collaboration, R. Barate *et al.*, Phys. Lett. **B465** (1999) 349.

Figure 1: Distributions of the most sensitive input variables of the vertex ANN at $\sqrt{s} = 183 - 189\,\mathrm{GeV}$: (a) decay length significance $L/\sigma_L$ and (b) primary vertex joint probability. Points with error bars represent the data (183 GeV and 189 GeV samples combined). Histograms represent the Monte Carlo expectation.
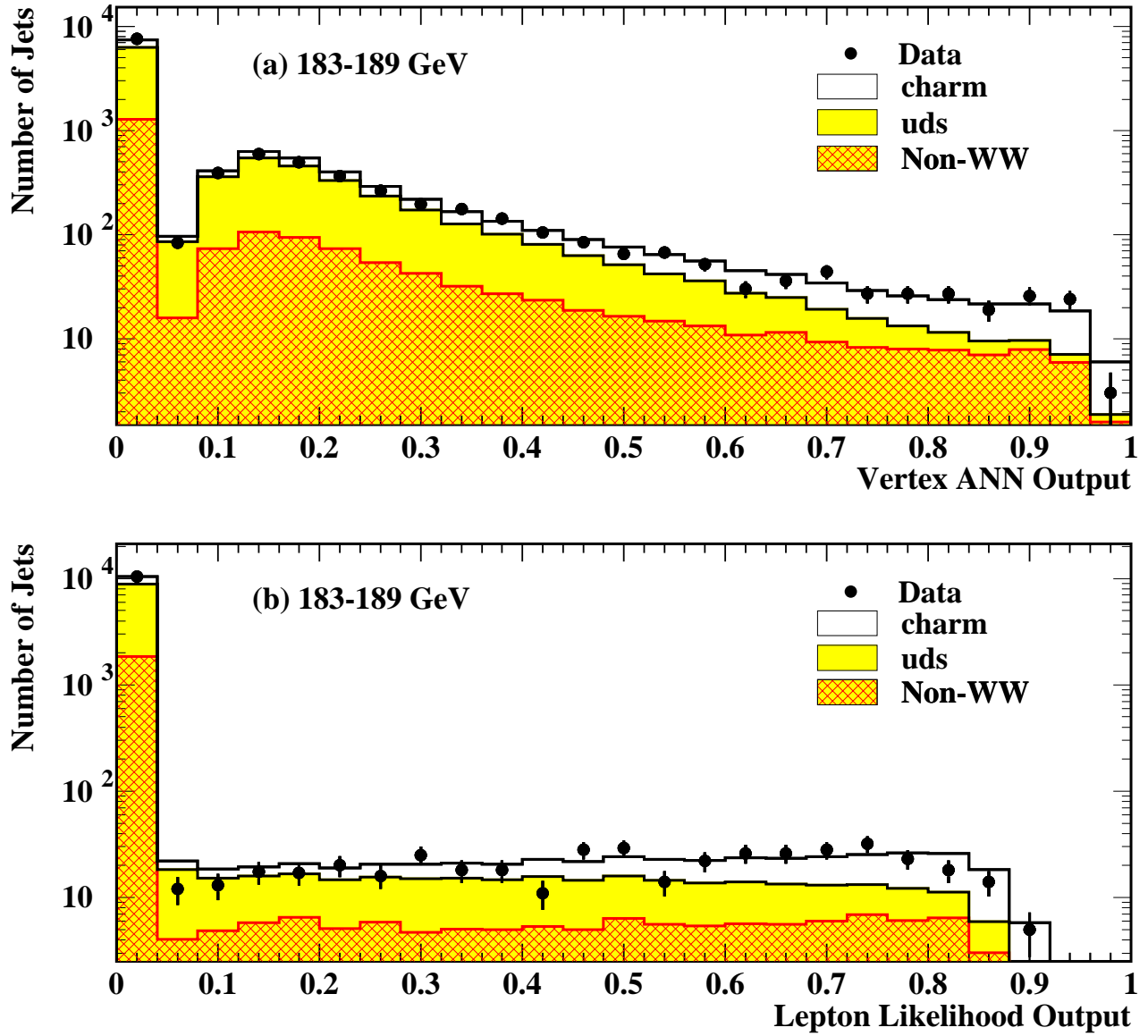
**OPAL**



Figure 2: Distributions of (a) the vertex ANN output and (b) the likelihood output of the lepton tag at $\sqrt{s} = 183 - 189\,\mathrm{GeV}$. Points with error bars represent the data ($183\,\mathrm{GeV}$ and $189\,\mathrm{GeV}$ samples combined). Histograms show the results of the fits to the combined likelihood described in Section 4.4. If no vertex or lepton tag information is available, the corresponding variable is assigned the value of zero.
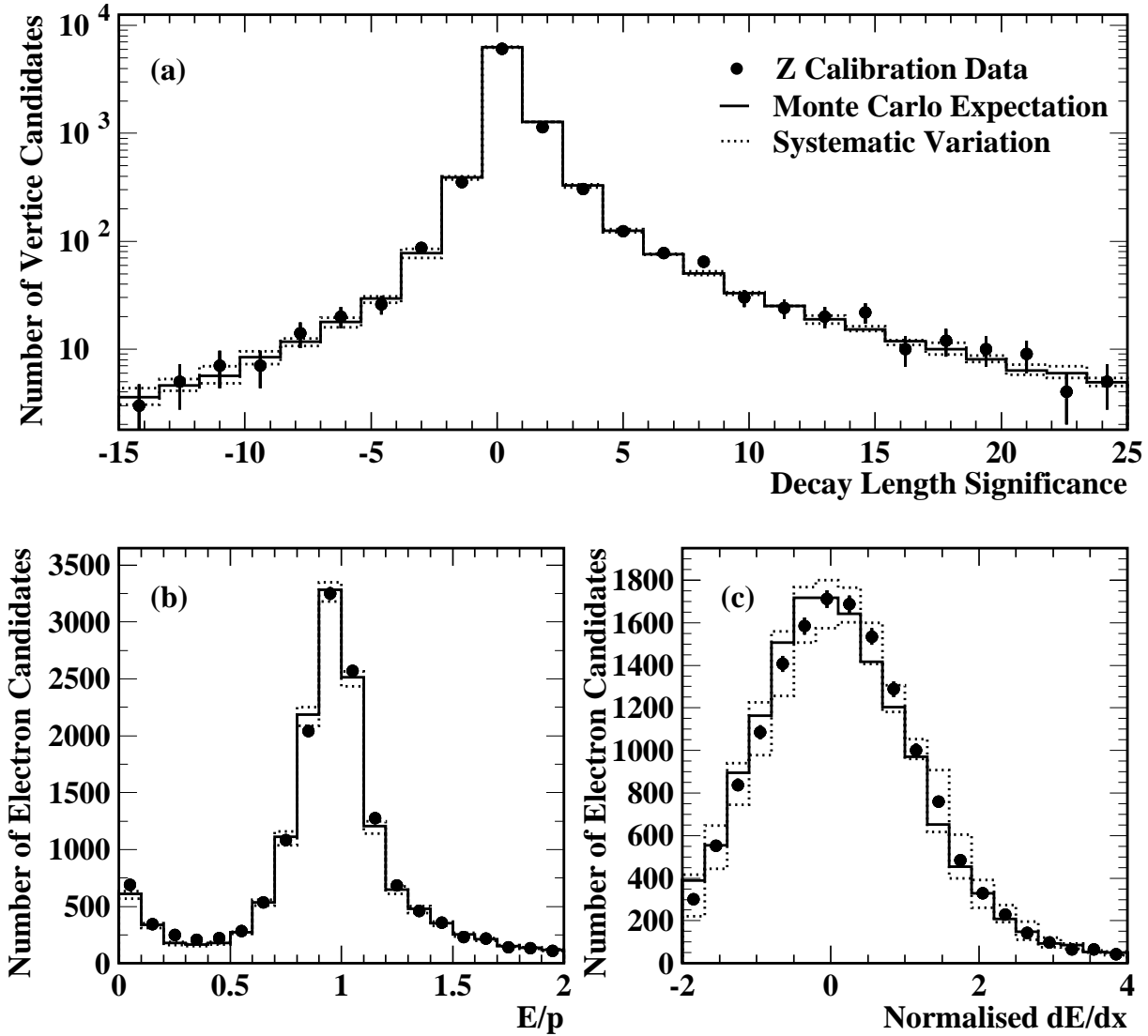
**OPAL**

Figure 3: Comparison of discriminating variables between calibration data taken at the $Z^0$ resonance and Monte Carlo prediction. Points with error bars represent data from the $Z^0$ calibration runs. Histograms show the expectation from the Monte Carole simulation. (a) Decay length significance $L/\sigma_L$ for data and Monte Carlo. The dotted line shows the effect of the $\pm 5\,\%$ variation of the tracking resolution used to assess the systematic uncertainty on the vertex tag. (b) $E/p$ and (c) normalised $dE/dx$ for electron candidates from data and Monte Carlo. In these plots, electrons must satisfy the pre-selection described in the text and have an electron ANN output greater than 0.5. The dotted lines show how the variation of the detection (mis)identification and resolution for electron candidates affects the $E/p$ and $dE/dx$ distributions.
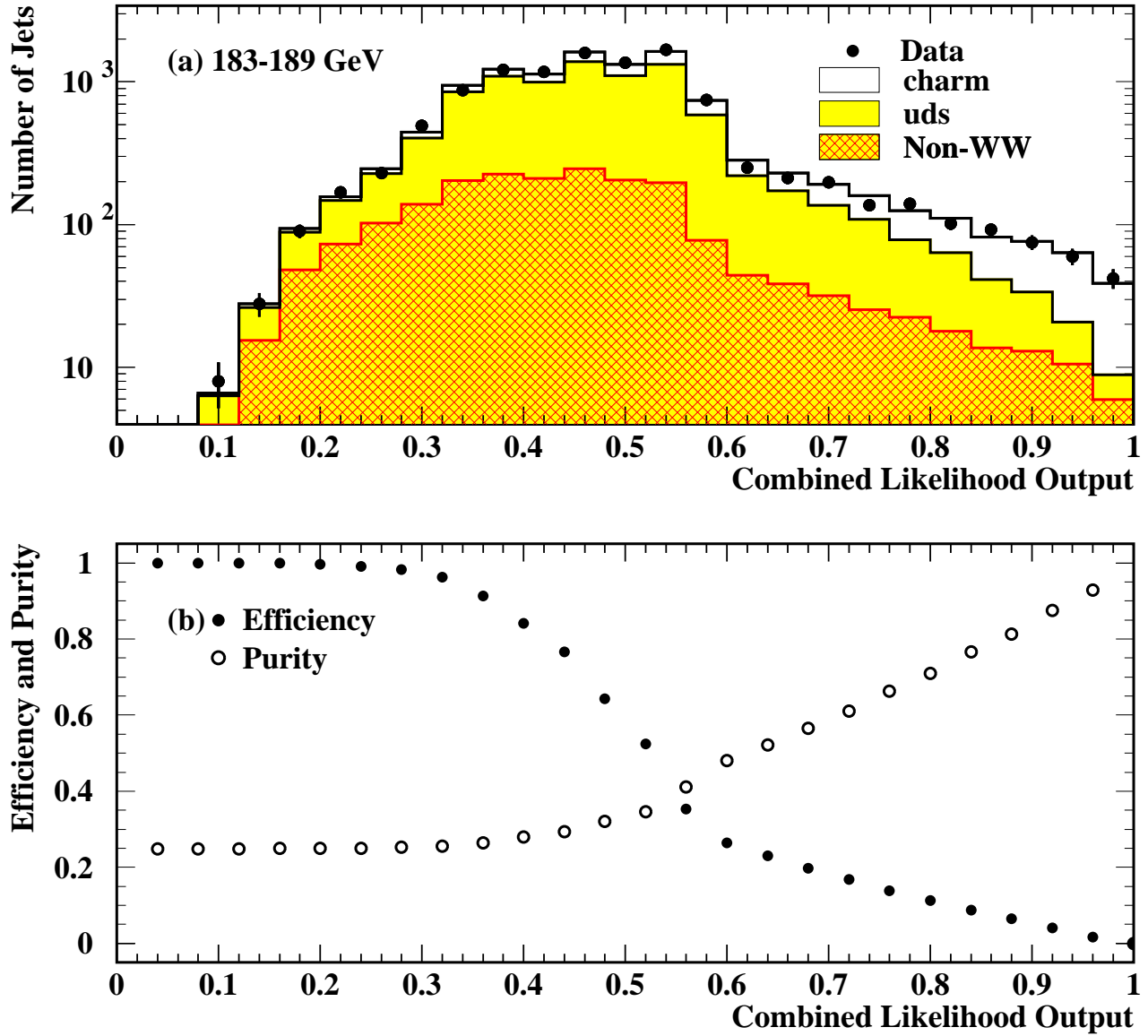
**OPAL**



Figure 4: (a) Output of the combined likelihood used to tag charm hadrons at $183 - 189\,\mathrm{GeV}$. Points with error bars represent the data ($183\,\mathrm{GeV}$ and $189\,\mathrm{GeV}$ samples combined). Histograms represent the results of the fits described in Section 4.4. (b) Efficiency and purity computed after the WW selection as a function of a cut on the combined likelihood output.